

MICROSTRUCTURAL ADAPTATIONS OF THE SUBCHONDRAL BONE ARE RELATED TO THE MECHANICAL AXIS DEVIATION IN END STAGE VARUS OA KNEES

W. Colyn^{1,2,3,§,*}, F. Azari^{4,§}, J. Bellemans^{2,5,6}, G.H. van Lenthe^{4,#} and L. Scheys^{7,#}

¹Department of Orthopaedic Surgery, AZ Turnhout, Turnhout, Belgium

²Faculty of Medicine and Life Sciences, Hasselt University, Diepenbeek, Belgium

³Limburg Clinical Research Centre, ZOL Genk, Belgium

⁴Biomechanics Section, KU Leuven, Leuven, Belgium

⁵Department of Orthopaedic Surgery, ZOL Genk, Genk, Belgium

⁶GRIT Belgian Sports Clinic, Leuven, Belgium

⁷Department of Orthopaedics, University Hospitals Leuven, Leuven, Belgium

[§] These authors equally contributed to this paper

[#] These authors equally contributed to this paper

Abstract

Recent studies highlighted the crucial contribution of subchondral bone to OA development. Yet, only limited data have been reported on the relation between alteration to cartilage morphology, structural properties of the subchondral bone plate (SBP) and underlying subchondral trabecular bone (STB). Furthermore, the relationship between the morphometry of the cartilage and bone in the tibial plateau and the OA-induced changes in the joint's mechanical axis remains unexplored. Therefore, a visualisation and quantification of cartilage and subchondral bone microstructure in the medial tibial plateau was performed. End stage knee-OA patients with varus alignment and scheduled for total knee arthroplasty (TKA) underwent preoperative full-length radiography to measure the hip-knee-ankle angle (HKA) and the mechanical-axis deviation (MAD). 18 tibial plateaux were μ -CT scanned (20.1 $\mu\text{m}/\text{voxel}$). Cartilage thickness, SBP, and STB microarchitecture were quantified in 10 volumes of interest (VOIs) in each medial tibial plateau. Significant differences ($p < 0.001$) were found for cartilage thickness, SBP, and STB microarchitecture parameters among the VOIs. Closer to the mechanical axis, cartilage thickness was consistently smaller, while SBP thickness and STB bone volume fraction (BV/TV) were higher. Moreover, trabeculae were also more superior-inferiorly oriented, *i.e.* perpendicular to the transverse plane of the tibial plateau. As cartilage and subchondral bone changes reflect responses to local mechanical loading patterns in the joint, the results suggested that region-specific subchondral bone adaptations were related to the degree of varus deformity. More specifically, subchondral sclerosis appeared to be most pronounced closer to the mechanical axis of the knee.

Keywords: Osteoarthritis, subchondral bone, tibial plateau, varus alignment, μ CT.

***Address for correspondence:** William Colyn, Orthopaedic Department, AZ Turnhout, Steenweg Op Merksplas 44, 2300 Turnhout, Belgium.

Telephone number: +32 1444 4675 Email: william_colyn@hotmail.com

Copyright policy: This article is distributed in accordance with Creative Commons Attribution Licence (<http://creativecommons.org/licenses/by/4.0/>).

List of Abbreviations

ANOVA	analysis of variance	ICC	intraclass correlation coefficient
BMI	body mass index	KL grade	Kellgren-Lawrence grade
BV/TV	bone volume fraction	LMM	linear mixed-effect models
Cart.Th	cartilage thickness	MA	mechanical axis
CIs	confidence intervals	MAD	mechanical axis deviation
DA	degree of anisotropy	MDC	minimum detectable change
HKA	hip-knee-ankle	MIL	mean intercept length
		MPTA	medial proximal tibial angle
		OA	osteoarthritis

sBMD	subchondral-bone mineral density
SBP	subchondral-bone plate
SBP.Po	subchondral-bone plate porosity
SBP.Th	subchondral-bone plate thickness
SD	standard deviation
SEM	standard error of measurement
SMI	structural model index
STB	subchondral trabecular bone
Tb.N	trabecular number
Tb.Or	trabecular orientation
Tb.Sp	trabecular separation
TKA	total knee arthroplasty
VOI	volume of interest
3D-PTO	3D principal trabecular orientation
μ CT	micro computed tomography

Introduction

Knee OA is a highly prevalent health problem that can lead to major physical disabilities. OA is typically characterised as a deterioration of the joint's cartilage (Alizai *et al.*, 2019; Sacitharan, 2019). However, more recent studies report this cartilage damage to be associated with significant changes of the subchondral bone microstructure (Holzer *et al.*, 2020; Rapagna *et al.*, 2021). These studies suggest that aberrant mechanical loading initiates a vicious cycle of subchondral bone loss, further followed by sclerosis, which in turn again further contributes to the progression of OA (Burr *et al.*, 2012; Holzer *et al.*, 2020). Importantly, such changes might affect the shock-absorbing properties of this subchondral bone (Roberts *et al.*, 2018).

On a micro scale, the STB microarchitecture is significantly affected in end-stage knee OA patients (Roberts *et al.*, 2018; Sharma *et al.*, 2001). Interestingly, these changes are related to knee joint loading indices.

As a subgroup of the OA population, constitutional varus subjects already present with a slight varus alignment from the end of growth onwards (Bellemans *et al.*, 2012), which is assumed to be associated with a more pronounced loading of the medial compartment of the knee. This pronounced loading would, in view of Wolff's law (Wolff, 1892), also lead to adaptations to the subchondral bone. Indeed, patients with varus alignment have a thinner cartilage layer, a thicker SBP and higher bone-volume fraction (Han *et al.*, 2020; Holzer *et al.*, 2020; Rapagna *et al.*, 2021; Roberts *et al.*, 2017; Roberts *et al.*, 2018; Wolff, 1892). With the onset of OA, a progressive overloading of the medial compartment can be expected to even further alter the subchondral bone microstructure in these constitutional varus subjects.

Using computed tomography (Omoumi *et al.*, 2015; 2017) demonstrated a higher sBMD and a less preserved cartilage in the medial-femorotibial compartment of OA knees. Most μ CT studies on functional bone adaptation in OA subjects have primarily focused on a comparison between the medial and lateral tibial compartment (Han *et al.*, 2020; Holzer *et al.*, 2020; Rapagna *et al.*, 2021; Roberts

et al., 2017; Roberts *et al.*, 2018). Consequently, regional differences within the medial tibial plateau remain largely unexplored in those studies. Yet, comparing regions throughout the medial-tibial plateau has the potential to better elucidate a potential relationship between OA-induced changes in the location and orientation of the MA of the knee and more localised microstructural changes in subchondral bone.

The aim of the current study was to quantify the subchondral bone microarchitecture throughout the medial-tibial plateau in subjects with end-stage knee OA with varus malalignment and to evaluate a possible relationship between their bone microstructure and the altered knee-joint alignment and loading axis. An increased varus alignment is associated with an increasing distance between the centre of the knee and the load-bearing axis, also defined as the MAD (see Fig. 1) (Colyn *et al.*, 2022).

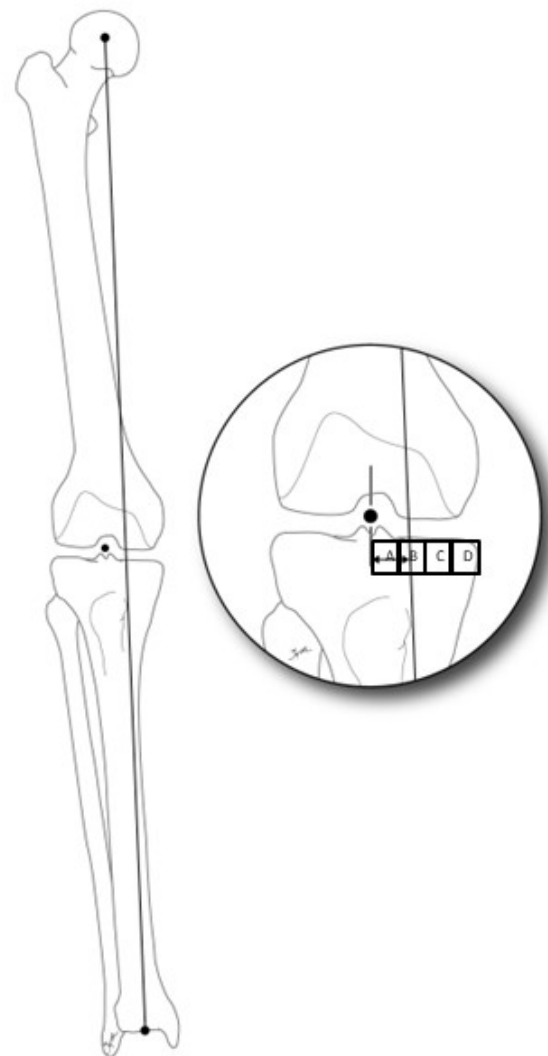


Fig. 1. Definitions of measurements. The MAD was defined as the distance between the centre of the knee and the MA line. The MA is determined as the line from the centre of the femoral head to the centre of the ankle. The insert illustrates that depending on the magnitude of the MAD it can be positioned in different VOIs (here illustrated by A,B,C and D).

It was hypothesised that as the VOI gets closer to the load bearing axis (Fig. 1), (1) the SBP thickness and the trabecular bone volume fraction will increase and (2) the predominant Tb.Or will be more aligned with the principal loading direction.

Materials and Methods

Specimens

This prospective study received approval from the ZOL Genk ethical committee (approval number of the project: B371201939696). Following informed consent, patients with end-stage knee OA KL grade (Kellgren and Lawrence, 1957) equal to 3 or 4 and scheduled for knee replacement surgery were included if they presented with a pre-operative varus malalignment above 5° based on the HKA-angle. HKA is defined as the angle between the mechanical axes of the femur and the tibia as measured on a full-length lower limb radiograph (Bellemans *et al.*, 2012). Patients presenting with a preoperative femoral or tibial fracture, osteotomy, any preceding ligamentous repair, or an ipsilateral total hip prosthesis were excluded. In total, 40 entire tibial plateau specimens were excised from included patients as part of their knee arthroplasty surgery. All surgeries were performed by one senior arthroplasty surgeon (William Colyn). The associated tibial cut was performed perpendicular to the mechanical tibial axis by using an intra-medullar guide. 22 specimens were excluded from further analysis because inspection revealed that the thickness of the medial condyle resulted in a STB layer of less than 3 mm, which would not allow for reliable measurement of bone microstructure (Harrigan *et al.*, 1998; Perilli *et al.*, 2015; Tassani and Perilli, 2013). A detailed summary of patients' characteristics for the 18 remaining specimens (7 males, 11 females, 10 right and 8 left knees) is given in Table 1. The specimens were preserved in a freezer at -20 °C, after they were rinsed and placed in a plastic bag.

Mechanical joint alignment

Full-leg radiographs were obtained with the patellae facing forward as part of routine clinical

care (Bellemans *et al.*, 2012). Following, a series of radiographic measurements were performed by one single rater (William Colyn) using the AGFA PACS software package (AGFA MIMOSA VIPS 1.3.00, Mortsel, Belgium). The femoral MA was defined as the line from the centre of the femoral head to the centre of the knee. The line from the centre of the knee to the centre of the ankle was defined as the tibial MA. 3 alignment parameters were measured: 1) The HKA-angle was formed by the mechanical femoral axis and the mechanical tibial axis. The HKA-angle was expressed as a deviation from 180° with a negative value for varus and positive value for valgus alignment. 2) The MAD was measured as the distance between the MA line and the centre of the knee. 3) The medial angle formed between the tibial MA and the knee joint line of the proximal tibia was defined as the MPTA (Bellemans *et al.*, 2012; Paley and Pfeil, 2000).

Subchondral bone microarchitecture

μCT imaging

μCT scans were performed in air using a desktop *μCT* scanner (Skyscan 1272, Bruker, Massachusetts, USA). Prior to scanning, the specimens were split into a medial and lateral condylar section through the eminentia tibiae, to fit into a 7 cm diameter *μCT* sample holder. The medial and lateral condyle of the specimens were wrapped in plastic film and fixed in

Table 1. Summary of patient characteristics. BMI = body mass index, MAD = mechanical axis deviation, HKA = Hip-knee-ankle angle, KL grade = Kellgren-Lawrence grade, MPTA = mechanical proximal tibial angle.

Parameters	End stage knee varus-OA, <i>n</i> = 18
Age	68.4 ± 5.8
BMI	30.9 ± 4.9
MAD	29.4 mm ± 10.9 mm
HKA	-8.2° ± 2.8°
KL Grade	3.2 ± 0.5
MPTA	86.5° ± 2.0°

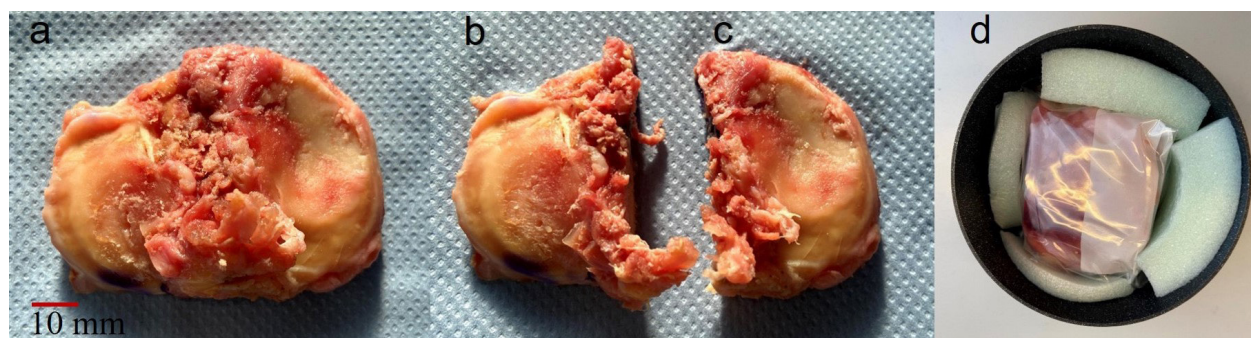


Fig. 2. Images of an included specimen. (a) complete tibial plateau, following separation in a (b) lateral condyle and (c) medial condyle, and (d) wrapped medial condyle mounted in the sample holder for *μCT* scanning.

the sample holder using mounting foam to prevent motion artefacts during scanning (Fig. 2). Each specimen was scanned using 100 kVp source voltage, 100 mA current, 0.4° rotation step, 180° rotation, 735 ms exposure time and 4-frames averaging. A 0.5 mm-thick aluminium-0.038 mm-thick copper filter was used for beam hardening artifact reduction.

The projection images were then reconstructed at 20.1 μm isotropic voxel size using a filtered back-projection algorithm (NRecon software; v1.7.5.2, Skyscan-Bruker) and saved as 8-bit images (256 gray-levels, bmp value of 0 = air, 255 = mineralised tissue). Prior to reconstruction, the CS rotation option in NRecon software was used to rotate the image stack such that its z-axis was aligned with the anatomical superior-inferior axis of each plateau based on visual inspection of the tibial cut. Representative coronal and transaxial views of μCT cross-sections are shown in Fig. 3.

Image segmentation

A 3D median filter ($\sigma = 3$) was applied to reduce noise in the images. Then, fixed global thresholding (87 grey value) was used to binarise the images in bony regions and air and marrow spaces, followed by further noise reduction using the despeckler function of CTAn software (1.19.4.0, Skyscan-Bruker). The medial condyle was subsequently categorised into three sub-regions: cartilage, SBP, and STB as described in more detail below.

Cartilage segmentation

A semi-automatic segmentation method was applied on the coronal image stack (Rapagna *et al.*, 2021). First, a negative mask was applied on the coronal image stack to exclude bone and marrow and identify cartilage and air in the images. Then, cartilage was specifically segmented by applying thresholding (87 grey value, CTAn software). The cartilage

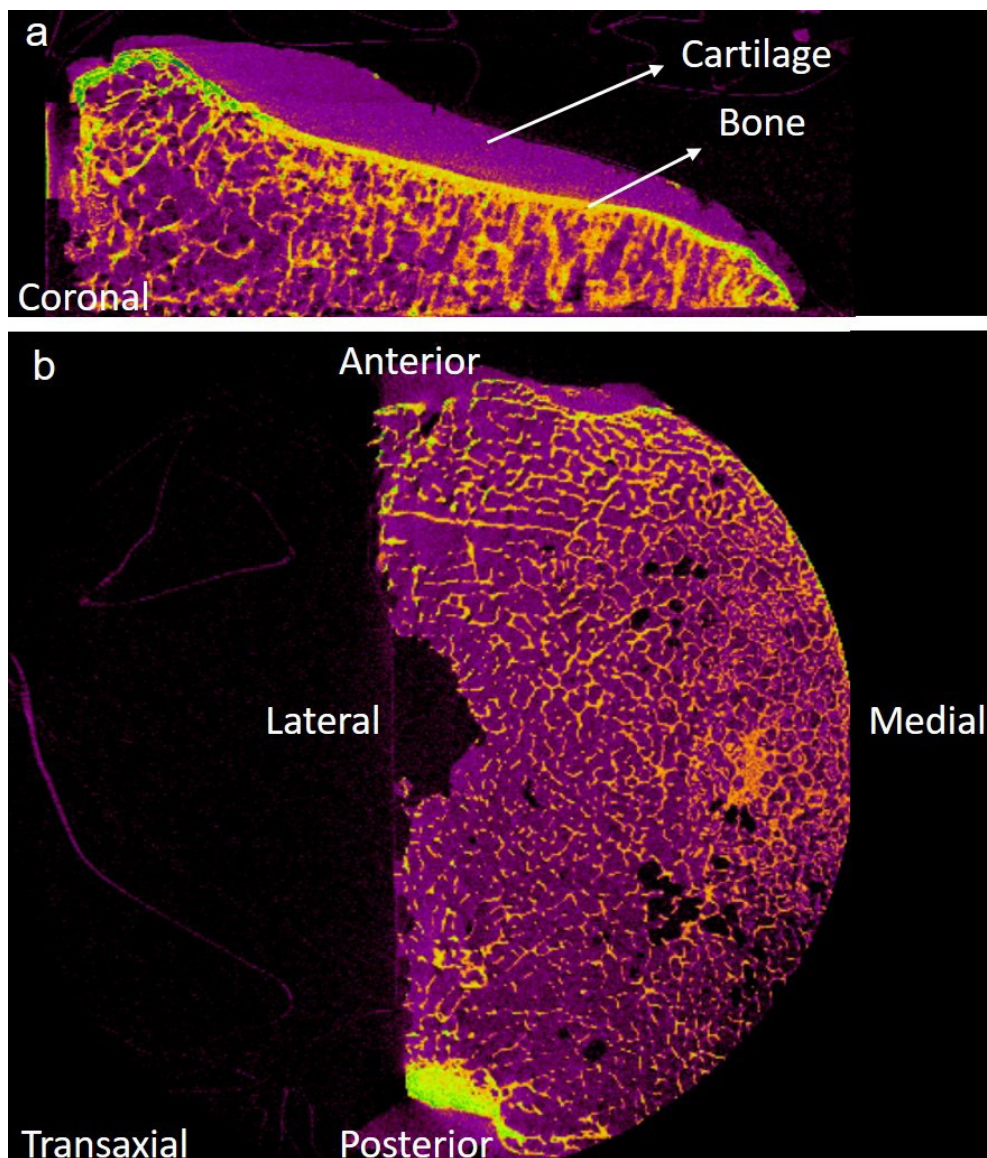


Fig. 3. Representative μCT cross-sectional images of a medial tibial condyle. Coronal view (a) and transaxial view (b), reconstructed at 20.1 μm isotropic voxel size. Segmented bone is highlighted in bright green colour, whereas segmented cartilage and bone marrow are shown in purple.

segmentation was visually inspected and manually corrected by indicating the cartilage boundaries every 10th coronal slice (0.20 mm) and subsequently interpolated for in-between images. Next, the “shrink-wrap” plug-in of CTAn was applied to automatically adjust the thresholding-based cartilage mask to these manually defined cartilage boundaries.

SBP segmentation from underlying STB

Manual contouring was performed to distinguish between SBP and STB. Specifically, SBP was separated from STB by contouring every 10th coronal slice (0.20 mm) and subsequent interpolation for in-between images (CTAn software). A representative 3D segmented model of a medial condyle is shown in Fig. 4.

VOIs definition

For each medial condyle, 13 cylindrical VOIs were defined for further analysis of cartilage, SBP, and STB. To ease interpretation of the data, these VOIs were grouped in four subgroups A,B,C,D (Fig. 5b), based on their central-to-lateral position, starting from the centre of the tibia. A second subdivision was made by subgrouping the VOIs from anterior (subgroup 1), through central (subgroup 2) to posterior (subgroup 3) (Fig 5b). Each cylindrical VOI measured 6 mm in diameter and VOIs were spaced with a medio-lateral and superior-inferior overlap of 1.3 mm. VOIs included a maximum of 5 mm of STB measured from

the inferior border of the SBP. When the height of the STB was less than 3 mm, the VOI was excluded from the analysis because in that case the STB does not satisfy the continuum assumption of trabecular bone for 3D morphometric analysis (Harrigan *et al.*, 1998; Tassani and Perilli, 2013). Upon further inspection, some specimens demonstrated signs of bone damage in the three most lateral VOIs (Fig. 5). This damage resulted from the intramedullary guide used during surgery to perform the tibial cut. Therefore, these VOIs were excluded from analysis for all specimens. For medio-lateral referencing, one additional VOI with equal dimensions (6 mm in diameter and 5 mm of STB) was positioned in the centre of the lateral condyle.

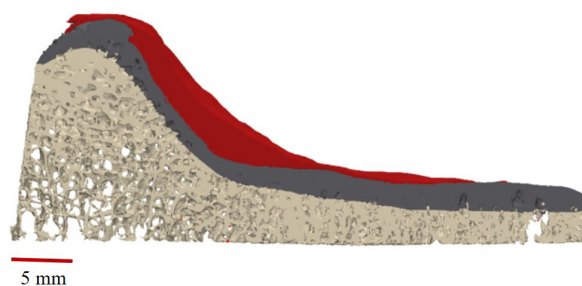


Fig. 4. Representative model of a segmented medial tibial condyle. The red layer represents the cartilage, the yellow layer represents the segmented SBP, and the brown layer represents the segmented STB.

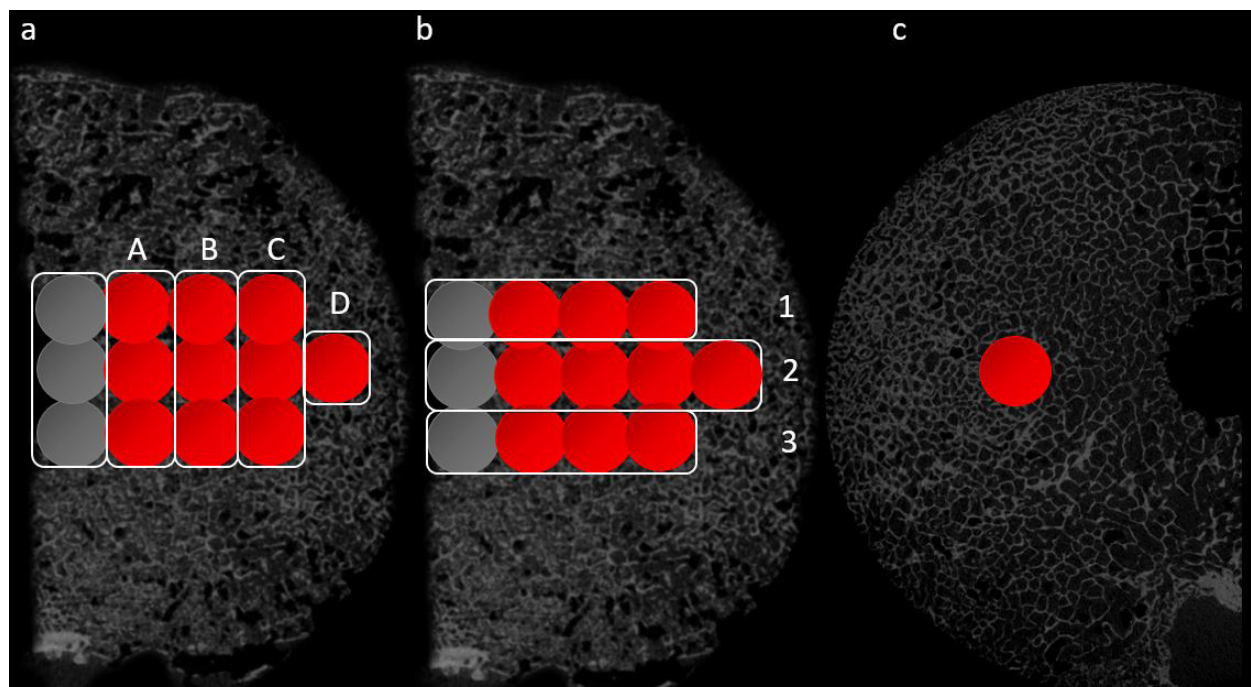


Fig. 5. VOI definition on representative μ CT cross-sectional images. Excised medial (a,b) and lateral condyle (c) from a right knee. Starting from the knee centre, 13 cylindrical VOIs were defined along the tibia’s medio-lateral axis with a 6 mm diameter and a medio-lateral overlap of 1.3 mm in the medial condyle. For quantitative analysis, the VOIs were grouped with respect to their anatomical location from central to medial (groups A-D) and from anterior to posterior (groups 1-3) in the medial condyle. VOIs shown in grey were excluded from the analysis because 15 specimens showed signs of bony damage related to the surgical procedure. One VOI with a 6 mm diameter was defined in the centre of the lateral condyle (c).

Morphometric analysis

All morphometric parameters were quantified using CTAn software. Cartilage thickness (Cart.Th, mm), average 3D thickness of the trabeculae (Tb.Th, μm), trabecular separation (Tb.Sp, μm), trabecular number (Tb.N, 1/mm), and SMI were calculated based on the sphere fitting method (Bouxsein *et al.*, 2010; Hildebrand and Rüegsegger, 1997). BV/TV was calculated as the ratio of the number of bone voxels to the total number of voxels in a given VOI (Dempster *et al.*, 2013). In the lateral condyle bone volume fraction (BV/TV)_{lat} was determined, too. Then, the normalised bone volume fraction (BV/TV*) was determined as (BV/TV) / (BV/TV)_{lat} to account for inter-individual differences. This approach is justified given that previous studies have demonstrated a uniform distribution of morphological parameters across the undamaged side of tibial plateaus in varus knees (Rapagna *et al.*, 2021; Roberts *et al.*, 2017). For the SBP within each VOI, SBP.Th and SBP.Po were calculated. SBP thickness (SBP.Th, mm) was calculated using the sphere-fitting method. SBP.Po was computed as the percentage of pore volume within the total tissue volume. Therefore, the number of voxels segmented as pore within the SBP VOI was divided by the total number of voxels inside the VOI. 3D-PTO and DA were determined using MIL analysis (CTAn software). Whereas DA is a measure of the homogeneity in terms of orientation within the VOI with a larger value indicating a more structured, dominant alignment. 3D-PTO provides the principal direction of the trabecular structure (Bouxsein *et al.*, 2010). Average values were calculated for all morphometric parameters and each subgroup: A,B,C,D as well as for anterior (subgroup 1), central (subgroup 2), and posterior (subgroup 3).

Statistics

The assumption of normality was tested and confirmed for all analysed variables using the Shapiro-Wilk test. Differences in morphometric parameters among the 10 regions throughout the medial condyle, based on their distance from MA location, were assessed using one-way repeated measures unbalanced ANOVA, followed by a Bonferroni-corrected *post hoc* test. The significance level was adjusted based on Bonferroni correction for multiple comparisons (significance level of 0.05 was modified to 0.001 with dividing by the number of tests). Correlations between leg length and MPTA for excluded specimens were examined using Pearson's correlation. MATLAB (R2019b, Mathworks, Massachusetts, United States) was used for all above mentioned statistical analyses.

LMM analysis was then performed using Rstudio (2021.09.1, RStudio, Boston, Massachusetts, United States) to investigate significant changes of BV/TV over A,B,C,D regions within specimens and to identify independent predictors of BV/TV. Hereto, the LMM was defined with BV/TV as outcome measure, with random effects for specimen ID and fixed effects for age, gender, KL grade, MPTA, HKA, BMI, and the individual distances from the VOIs A, B, C, D to the MA.

To assess the intra-rater reliability of the image-based manual measurements, one operator repeated the measurements and the ICC was determined (Koo and Li, 2016; Shrout and Fleiss, 1979) using Rstudio (2021.09.1, RStudio, Boston, Massachusetts, United States). Likewise, the inter-rater reliability was assessed by evaluating the ICC for outcomes of two mutually blinded operators. The following ICC parameters were used to analyse the radiographical

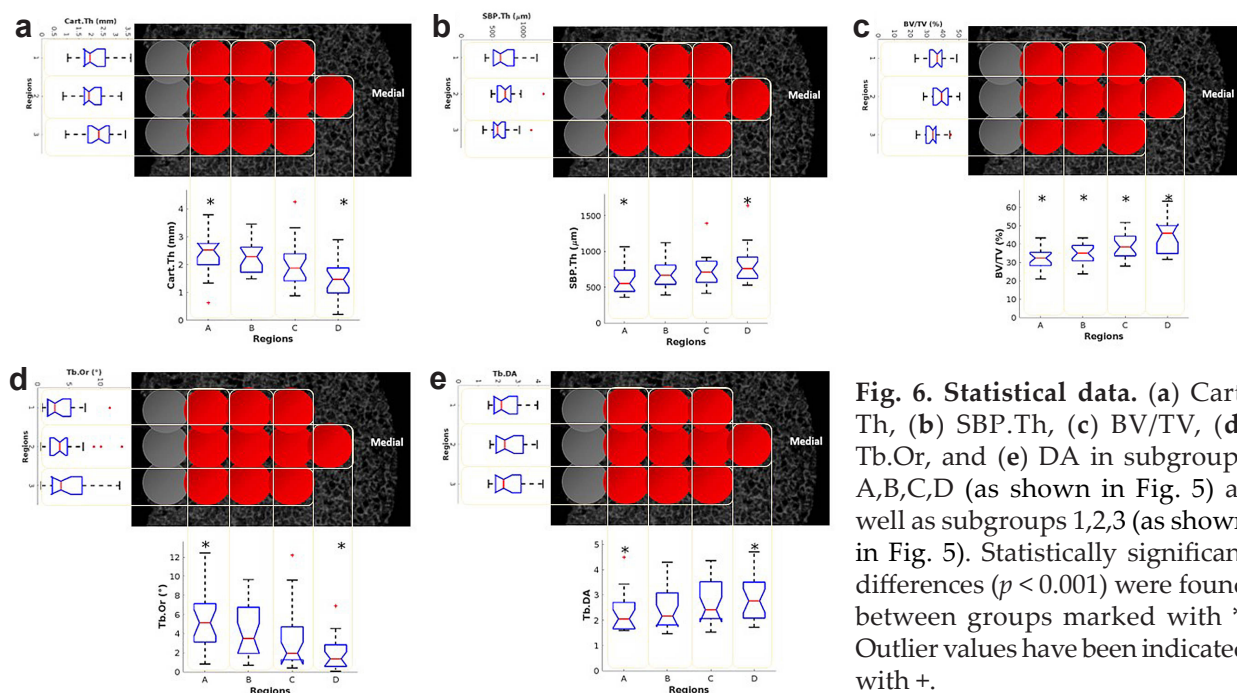


Fig. 6. Statistical data. (a) Cart. Th, (b) SBP.Th, (c) BV/TV, (d) Tb.Or, and (e) DA in subgroups A,B,C,D (as shown in Fig. 5) as well as subgroups 1,2,3 (as shown in Fig. 5). Statistically significant differences ($p < 0.001$) were found between groups marked with *. Outlier values have been indicated with +.

measurements for HKA, MAD, and MPTA: two-way model, two raters for 18 samples, type: absolute agreement. The following ICC parameters were used to evaluate μ CT contouring for SBP thickness and SBP porosity: two-way model, two raters for 17 samples, type: absolute agreement. All ICCs were interpreted according to Koo and Li (Koo and Li, 2016) (0.0-0.5 poor; 0.5-0.75 moderate, 0.75-0.9 good, 0.9-1.0 excellent). SEM and MDC were calculated.

Results

Location of the MA

In all specimens the VOI closest to MA is VOI D except for one specimen in which the MA is located in VOI C.

Cartilage morphometry

The average Cart.Th over all 10 VOIs was 2.1 ± 0.6 mm. No differences were found in Cart.Th across subgroups 1,2,3, while cartilage was found to be significantly thinner ($p < 0.001$) in VOI D than subgroup A (Fig. 6a).

Bone morphometry

The SBP had an average thickness of 692.1 ± 187.9 μ m over all VOIs, with no differences being found among subgroups 1,2,3. SBP.Th was however significantly higher ($p < 0.001$) in VOI D than subgroup A (Fig. 6b, $p < 0.001$). Also, BV/TV was significantly higher ($p < 0.001$) in VOI D than subgroup A (Fig. 6c, $p < 0.001$) with an average value of 36.7 ± 5.6 % over all VOIs and with no significant differences occurring between subgroup 1,2,3. In VOI D trabeculae orientation was closer to zero hence significantly more aligned with the vertical direction ($p < 0.001$) than subgroup A (Fig. 6d). Also, significantly greater trabecular anisotropy ($p < 0.001$) was observed in VOI D than subgroup A (Fig. 6e). Statistical analysis also showed Tb.Th and Tb.N were significantly higher in VOI D than subgroup A ($p < 0.001$; Table 2), whereas SBP.Po, SMI, and Tb.Sp were significantly lower in VOI D than subgroup A ($p < 0.001$; Table 2).

Association between bone volume fraction and distance from MA

BV/TV was on average 50 ± 4.6 % higher in the medial condyle with the average of 36.2 ± 5.6 % than in the lateral condyle with the average of 24.1 ± 4.9 %. The

Table 2. Mean \pm SD of cartilage and bone morphometric parameters in ten VOIs in medial condyle and in one VOI of lateral condyle. The VOIs were grouped in four subgroups A,B,C,D based on their central-to-lateral position, starting from the centre of the tibia. A second subdivision was made by subgrouping the VOIs from anterior (subgroup 1), through central (subgroup 2) to posterior (subgroup 3). One additional VOI was positioned in the centre of the lateral condyle.

VOI	Morphometric parameters. Mean \pm SD							
	Cart.Th (mm)	SBP.Th (μ m)	SBP.Po (%)	BV/TV (%)	Tb.Th (μ m)	Tb.Sp (μ m)	Tb.N (1/mm)	SMI
VOI A1	2.3 \pm 0.8	679 \pm 279	8.7 \pm 3.3	34.2 \pm 6.6	217 \pm 33	491 \pm 123	1.4 \pm 0.3	1.2 \pm 0.7
VOI B1	2.2 \pm 0.6	695 \pm 193	8.3 \pm 4.9	35.8 \pm 6.4	233 \pm 42	447 \pm 116	1.6 \pm 0.3	0.9 \pm 0.9
VOI C1	1.9 \pm 0.9	739 \pm 189	7.7 \pm 4.7	38.3 \pm 9.1	237 \pm 57	423 \pm 145	2.7 \pm 0.4	0.7 \pm 1.3
VOI A2	2.4 \pm 0.9	802 \pm 247	9.6 \pm 3.2	34.3 \pm 3.7	247 \pm 46	480 \pm 110	1.3 \pm 0.2	1.2 \pm 0.5
VOI B2	2.3 \pm 0.6	663 \pm 281	8.2 \pm 3.8	35.3 \pm 6.6	225 \pm 40	471 \pm 150	1.6 \pm 0.3	0.9 \pm 0.7
VOI C2	2.0 \pm 0.9	700 \pm 245	7.9 \pm 3.4	40.2 \pm 8.3	240 \pm 58	400 \pm 107	1.8 \pm 0.3	0.3 \pm 1.0
VOI D	1.4 \pm 0.7	742 \pm 242	7.8 \pm 2.7	44.8 \pm 10.3	245 \pm 63	370 \pm 99	2.0 \pm 0.5	0.1 \pm 0.4
VOI A3	2.4 \pm 0.7	576 \pm 175	9.6 \pm 3.7	30.0 \pm 6.2	234 \pm 36	538 \pm 139	1.3 \pm 0.4	1.4 \pm 0.4
VOI B3	2.4 \pm 0.7	628 \pm 185	8.8 \pm 4.4	33.1 \pm 6.2	237 \pm 34	505 \pm 118	1.4 \pm 0.3	1.1 \pm 0.5
VOI C3	2.1 \pm 0.7	693 \pm 219	7.6 \pm 4.0	37.6 \pm 7.0	244 \pm 49	430 \pm 124	1.7 \pm 0.3	0.7 \pm 0.7
Lateral VOI	3.0 \pm 0.7	548 \pm 164	11.0 \pm 3.0	24.1 \pm 4.9	177 \pm 30	531 \pm 66	1.4 \pm 0.3	1.3 \pm 0.4
Subgroup A	2.4 \pm 0.7	607 \pm 205	9.1 \pm 2.9	31.7 \pm 5.4	229 \pm 35	507 \pm 124	1.4 \pm 0.3	1.0 \pm 0.6
Subgroup B	2.3 \pm 0.6	675 \pm 193	8.4 \pm 3.5	34.7 \pm 5.5	232 \pm 33	474 \pm 109	1.5 \pm 0.3	0.8 \pm 0.5
Subgroup C	2.0 \pm 0.8	725 \pm 207	7.7 \pm 3.8	38.7 \pm 7.4	240 \pm 47	418 \pm 118	1.7 \pm 0.3	0.5 \pm 0.3
Subgroup D	1.4 \pm 0.7	802 \pm 247	7.8 \pm 4.4	44.8 \pm 10.3	245 \pm 63	370 \pm 99	2.0 \pm 0.5	0.9 \pm 0.6
Subgroup 1	2.1 \pm 0.7	696 \pm 232	8.3 \pm 3.0	35.8 \pm 6.5	231 \pm 40	446 \pm 117	1.6 \pm 0.3	0.7 \pm 0.5
Subgroup 2	2.0 \pm 0.6	732 \pm 195	8.1 \pm 3.4	38.6 \pm 6.6	236 \pm 42	431 \pm 94	1.7 \pm 0.3	0.9 \pm 0.5
Subgroup 3	2.3 \pm 0.6	627 \pm 183	8.5 \pm 3.8	33.5 \pm 5.6	237 \pm 34	494 \pm 117	1.5 \pm 0.3	1.1 \pm 0.5

linear mixed model for BV/TV identified the distance from the MA (the individual distances from the VOIs A,B,C,D to the MA) and BMI as the only two factors to be significantly affecting BV/TV (adjusted $R^2 = 0.88$). The effect of the distance from the MA and BMI appeared to be strong ($p < 0.001$), but the large SD (64 %) indicated strong inter-individual differences. The effect of the distance from the MA and BMI with normalised data was further increased ($p < 0.001$) while the SD reduced to 48 %, indicating the presence of additional sources of inter-individual differences affecting this relation.

Reliability analyses

Results of the intra- and inter-rater reliability analyses are summarised in Table 3. The intra- and inter-rater reliability were excellent for the MPTA, HKA and MAD parameters ($ICC \geq 0.93$, $p < 0.001$, $SEM \leq 0.065$, and $MDC \leq 0.709$). Likewise, the measurements of SBP thickness and porosity both displayed excellent intra- and inter-rater repeatability ($ICC \geq 0.91$, $p < 0.001$, $SEM \leq 0.002$, and $MDC \leq 0.132$).

Discussion

The most important finding of this study was that in end stage OA knees with varus malalignment the articular cartilage and localised subchondral bone changes in the medial tibial plateau were related to the joint alignment and its distance to the loading axis. Specifically, the Cart.Th was thinner closer to the MA. In contrast, the SBP.Th as well as its trabecular volume fraction was found to increase through the medial plateau as the distance to the MA reduced. Furthermore, in VOI D trabeculae orientation was closer to zero, hence more aligned with the vertical direction than subgroup A and a greater trabecular anisotropy was observed in the more medial VOIs.

Prior studies already described changes in the overall subchondral bone structure of the medial *versus* the lateral compartment (Han *et al.*, 2020; Holzer *et al.*, 2020; Rapagna *et al.*, 2021; Roberts *et al.*, 2017; Roberts *et al.*, 2018). However, as far as is known, this study was the first to evaluate microstructural differences in cartilage and subchondral bone within the medial plateau. Furthermore, it was the first to demonstrate that these microstructural changes are

Table 3. Intra- and inter-rater reliability of the manual measurements. ICCs were calculated with “absolute agreement,” and the results were given with their 95 % CIs. Colour codes indicate ICC reliability (poor < 0.5; 0.5 < moderate < 0.75; blue: 0.75 < good < 0.9; green: 0.9 < excellent). SEM and MDC were reported.

	ICC	95% CI	SEM	MDC
Intraobserver comparison (1 observer, 2 trials)				
MPTA				
HKA	0.95	0.88-0.98	0.057	0.664
MAD	0.99	0.98-0.99	0.013	0.319
SBP.Th	0.99	0.97-0.99	0.081	0.790
SBP.Po	0.98	0.96-0.99	0.037	0.535
BV/TV	0.96	0.90-0.99	0.002	0.115
Tb.Th	1.00	1.00-1.00	0.000	0.000
Tb.Sp	1.00	1.00-1.00	0.000	0.000
Tb.N	1.00	1.00-1.00	0.000	0.000
SMI	1.00	1.00-1.00	0.000	0.000
Interobserver comparison (2 observers)				
MPTA	0.93	0.86-0.97	0.065	0.709
HKA	0.99	0.98-0.99	0.010	0.271
MAD	0.99	0.98-0.99	0.062	0.689
SBP.Th	0.98	0.96-0.99	0.157	1.097
SBP.Po	0.91	0.77-0.97	0.002	0.132
BV/TV	1.00	1.00-1.00	0.000	0.000
Tb.Th	1.00	1.00-1.00	0.000	0.000
Tb.Sp	1.00	1.00-1.00	0.000	0.000
Tb.N	1.00	1.00-1.00	0.000	0.000
SMI	1.00	1.00-1.00	0.000	0.000

associated with the MA location and its alterations in end-stage OA knees with varus malalignment.

For the neutral knee, where the MA passes through the centre of the knee, a uniform distribution of cartilage across the plateau has been reported (Rapagna *et al.*, 2021). However, in varus knees, the MA is shifted medially, such that more pronounced varus knees will have larger MADs. Hence, the typical epicentre of the compressive load, associated with the location of the load-bearing axis, is progressively shifting medially during the arthritic process (Colyn *et al.*, 2022; Colyn *et al.*, 2023; Eckstein *et al.*, 2008;). It was also found that the Cart.Th in the medial plateau was consistently thinner than in the lateral plateau. Furthermore, the Cart.Th over 4 medio-lateral regions across the medial plateau was consistently thinner in the more medial VOIs ($p < 0.005$).

The findings of the current study corroborate prior studies that related mechanical loading to subchondral bone changes and OA progression (Burr *et al.*, 2003; Holzer *et al.*, 2020). Likewise, the current study confirmed earlier studies reporting that an increase in varus angle and OA correlates with more sclerosis in the medial compartment (Han *et al.*, 2020; Rapagna *et al.*, 2021; Roberts *et al.*, 2018). However, those studies only compared one single VOI in the medial portion of the tibial plateau to one single VOI in the lateral portion. By subdividing the medial portion of the tibia plateau into smaller VOIs, more localised changes were identified within the medial compartment in terms of the degree of sclerosis changes. Furthermore, sclerosis was more pronounced closer to the load-bearing axis. In line with prior studies, this sclerosis was characterised by an increased SBP.Th, trabecular bone volume fraction, trabecular thickness, trabecular number, and a decreased trabecular separation (Burr *et al.*, 2003; Rapagna *et al.*, 2021; Roberts *et al.*, 2018). This STB densification during OA has been suggested to be associated with a reduction in its elastic modulus, which could accelerate cartilage loss (Fell *et al.*, 2019; Reina *et al.*, 2017). Indeed, in the present study it was found that SBP.Th, trabecular bone volume fraction, trabecular thickness and trabecular number were associated with a thinner cartilage layer.

Interestingly, it was also found that the trabeculae orientation differed among the VOIs. As previously suggested by Ding *et al.* (2003) and Sampath *et al.* (2015), the current study seems to confirm a correlation between the Tb.Or and the MA. The trabeculae were directed towards the MA, whereby trabeculae closer to the MA were more aligned with the longitudinal direction. Further, the anisotropy has also been suggested to change in OA knees (Ding *et al.*, 2003; Sampath *et al.*, 2015; Wolski *et al.*, 2010); indeed, greater trabecular anisotropy was observed in the more medial VOIs. This can be explained by Wolff's Law, stating that the trabecular bone architecture follows the principal stress trajectories generated by external loads (Barak *et al.*, 2011). Furthermore,

by linking the above changes to the MA deviation as an indicator of the coronal load distribution, the current study provided some indications on how subchondral bone adapts to the changing loads during the arthritic process. Those bone adaptations are accepted as a concept of functional adaptation, that links mechanical loading to the bone structure (King *et al.*, 2007).

Finally, as the changes mentioned above also correlate with an increasing load, it was hypothesised that a correlation exists between the degree of subchondral bone remodelling and the patient's body weight. This hypothesis was confirmed. This is in line with the findings of Reina *et al.* (2017), who also identified a correlation between microstructural subchondral changes and BMI. Interestingly, neither age, gender, KL grade, MPTA, or HKA were found to further explain subchondral bone microstructure significantly within the study sample.

There were some limitations to the current study. First, with 18 cases the sample size was limited. Although a total of 40 tibial plateaux were collected, 22 specimens were excluded because the STB layer was too small to allow for an unbiased morphological analysis. To evaluate potential exclusion bias, the analyses were extended. 6 specimens were excluded, and a one-way repeated unbalanced ANOVA, followed by a Bonferroni-corrected *post hoc* test were used to evaluate Cart.Th, SBP.Th, and SBP.Po. Importantly, *Post-hoc* inclusion of these samples did not change any of the findings, indicating that there was no evidence of exclusion bias. Furthermore, leg length and MPTA were not found to correlate with specimen thickness ($r = 0.31$, $p = 0.20$). This provided further support for the view that there is no evidence of exclusion bias with regards to these input parameters when eliminating the specimens with a thickness less than 3 mm.

A second limitation was that only varus knees were studied. Valgus alignment was not investigated; therefore, whether similar variations were also present in valgus cases could not be determined. Furthermore, all patients had end-stage knee OA; hence, future research should elucidate to what extent the findings reported here can be extrapolated to the earlier stages of OA onset and progression. Moreover, it would be interesting to also include valgus patients in a follow-up study.

The intra- and inter-rater reliability of the measurements of the radiographs were excellent ($ICC \geq 0.93$, $p \ll 0.001$, $SEM \leq 0.065$, and $MDC \leq 0.709$). In addition, the evaluation of the μ CT-based microstructural properties showed high reliability ($ICC \geq 0.91$, $p \ll 0.001$, $SEM \leq 0.002$, and $MDC \leq 0.132$). This was in line with the notion that manual contouring is considered the gold standard for SBP segmentation (Perilli *et al.*, 2015; Rapagna *et al.*, 2021; Roberts *et al.*, 2017). Yet, manual contouring is time-consuming and remains a potential source of error. In order to mitigate this, Gatenholm *et al.* (2019) have

developed an automated segmentation process which reduces processing time and can take away some ambiguity in manual contouring.

As the third limitation, this study did not aim to answer the question whether cartilage thinning precedes subchondral bone changes, or whether it is the other way around. To answer this question, further investigation is needed to track the changes during OA progression, and not only evaluate end stage OA. Furthermore, further insight is required into understanding the role of the osteocyte network and the corresponding mechanosensory ability of subchondral bone in bone and cartilage remodelling during OA progression.

Future work will aim to use this study's findings to analyse the stability of conventional knee arthroplasty designs in end stage varus aligned OA knees. As the current study demonstrated that this group presents with a non-homogenic subchondral bone support, this could identify opportunities to optimise implant fixation and stability, specifically of the medial tibial plateau, when performing an arthroplasty through subject-specific alignment strategies that take such inhomogeneities into account. More specifically, such research could provide further scientific evidence with regards to the current clinical trend to place the tibial component in a slightly varus position (Nedopil *et al.*, 2017; Rivière *et al.*, 2022). Furthermore, future studies will aim to quantify the structural bone and cartilage morphology in the femoral compartment and investigate whether cartilage morphology and bone microstructure in the medial tibial plateau is associated with those of medial femur in end-stage OA.

Conclusions

Localised subchondral bone changes in the medial compartment are related to the distance to the load-bearing axis in end-stage OA varus knees. The Cart. Th was thinner closer to the load-bearing axis. In contrast, the SBP.Th was thicker, the trabecular bone volume fraction was higher, and the trabeculae were oriented more longitudinally close to the MA.

Acknowledgments

Author contributions

Study concept and design: Colyn, Bellemans, Van Lenthe, Scheys; Data acquisition: Colyn, Azari; Statistical analysis: Azari; Data Interpretation: all; Manuscript preparation: Colyn, Azari; Revision of Manuscript drafts: all.

Funding

This study was part of Limburg Clinical Research Centre supported by Hasselt University, Ziekenhuis Oost-Limburg and Jessa Hospital and was funded

in part by KU Leuven Internal Funds, Grant C24/16/027".

Conflict of interest

The authors declare to have no conflict of interests.

Ethical approval

Approval for this study was obtained by the Ethical Committee at ZOL Genk (19/0015U, B-nr: B371201939696).

References

- Alizai H, Walter W, Khodorahmi I, Burke CJ (2019) Cartilage imaging in osteoarthritis. *Semin Musculoskelet Radiol* **23**: 569-578. DOI: 10.1055/s-0039-1695720.
- Barak MM, Lieberman DE, Hublin JJ (2011) A Wolff in sheep's clothing: trabecular bone adaptation in response to changes in joint loading orientation. *Bone* **49**: 1141-1151. DOI: 10.1016/j.bone.2011.08.020.
- Bellemans J, Colyn W, Vandenuecker H, Victor J (2012) The Chitranjan Ranawat award: is neutral mechanical alignment normal for all patients? The concept of constitutional varus. *Clin Orthop Relat Res* **470**: 45-53. DOI: 10.1007/s11999-011-1936-5.
- Bouxsein ML, Boyd SK, Christiansen BA, Guldberg RE, Jepsen KJ, Müller R (2010) Guidelines for assessment of bone microstructure in rodents using micro-computed tomography. *J Bone Miner Res* **25**: 1468-1486. DOI: 10.1002/jbmr.141.
- Burr DB, Gallant MA (2012) Bone remodelling in osteoarthritis. *Nat Rev Rheumatol* **8**: 665-673. DOI: 10.1038/nrrheum.2012.130.
- Burr DB, Radin EL (2003) Microfractures and microcracks in subchondral bone: are they relevant to osteoarthritis? *Rheum Dis Clin North Am* **29**: 675-685. DOI: 10.1016/s0889-857x(03)00061-9.
- Colyn W, Bruckers L, Scheys L, Truijen J, Smeets K, Bellemans J (2023) Changes in coronal knee-alignment parameters during the osteoarthritic process in the varus knee. *J ISAKOS* **S2059-7754**: 00115-8. DOI: 10.1016/j.jisako.2022.12.002.
- Colyn W, Cleymans A, Bruckers L, Truijen J, Smeets K, Bellemans J (2022) The pre-diseased coronal alignment can be predicted from conventional radiographs taken of the varus arthritic knee. *Arch Orthop Trauma Surg*. DOI:10.1007/s00402-022-04709-6.
- Dempster DW, Compston JE, Drezner MK, Glorieux FH, Kanis JA, Malluche H, Meunier PJ, Ott SM, Recker RR, Parfitt AM (2013) Standardized nomenclature, symbols, and units for bone histomorphometry: a 2012 update of the report of the ASBMR Histomorphometry Nomenclature Committee. *J Bone Miner Res* **28**: 2-17. DOI: 10.1002/jbmr.1805.
- Ding M, Odgaard A, Hvid I (2003) Changes in the three-dimensional microstructure of human tibial

cancellous bone in early osteoarthritis. *J Bone Joint Surg Br* **85**: 906-912.

Eckstein F, Wirth W, Hudelmaier M, Stein V, Lengfelder V, Cahue S, Marshall M, Prasad P, Sharma L (2008) Patterns of femorotibial cartilage loss in knees with neutral, varus, and valgus alignment. *Arthritis Rheum* **59**: 1563-1570. DOI: 10.1002/art.24208.

Fell NLA, Lawless BM, Cox SC, Cooke ME, Eisenstein NM, Shepherd DET, Espino DM (2019) The role of subchondral bone, and its histomorphology, on the dynamic viscoelasticity of cartilage, bone and osteochondral cores. *Osteoarthritis Cartilage* **27**: 535-543. DOI: 10.1016/j.joca.2018.12.006.

Gatenholm B, Lindahl C, Brittberg M, Stadelmann VA (2019) Spatially matching morphometric assessment of cartilage and subchondral bone in osteoarthritic human knee joint with micro-computed tomography. *Bone* **10**: 393-402. DOI: 10.1016/j.bone.2018.12.003.

Han X, Cui J, Xie K, Jiang X, He Z, Du J, Chu L, Qu X, Ai S, Sun Q, Wang L, Wu H, Zhang W, Yu Z, Yan M (2020) Association between knee alignment, osteoarthritis disease severity, and subchondral trabecular bone microarchitecture in patients with knee osteoarthritis: a cross-sectional study. *Arthritis Res Ther* **22**: 203. DOI: 10.1186/s13075-020-02274-0.

Harrigan TP, Jasty M, Mann RW, Harris WH (1998) Limitations of the continuum assumption in cancellous bone. *J Biomech* **21**: 269-275. DOI: 10.1016/0021-9290(88)90257-6.

Hildebrand T, Rügsegger P (1997) Quantification of bone microarchitecture with the structure model index. *Comput Methods Biomech Biomed Engin* **1**: 15-23. DOI: 10.1080/01495739708936692.

Holzer LA, Kraiger M, Talakic E, Fritz GA, Avian A, Hofmeister A, Leithner A, Holzer G (2020) Microstructural analysis of subchondral bone in knee osteoarthritis. *Osteoporos Int* **31**: 2037-2045. DOI: 10.1007/s00198-020-05461-6.

Kellgren JH, Lawrence JS (1957) Radiological assessment of osteo-arthrosis. *Ann Rheum Dis* **4**: 494-502. DOI: 10.1136/ard.16.4.494.

King TE, Bowden GR, Balaresque PL, Adams SM, Shanks ME, Jobling MA (2007) Thomas Jefferson's Y chromosome belongs to a rare European lineage **9**: 584-589. DOI: 10.1002/ajpa.20557.

Koo TK, Li MY (2016) A guideline of selecting and reporting intraclass correlation coefficients for reliability research. *J Chiropr Med* **15**: 155-163. DOI: 10.1016/j.jcm.2016.02.012.

Nedopil AJ, Howell SM, Hull ML (2017) What mechanisms are associated with tibial component failure after kinematically-aligned total knee arthroplasty? *Int Orthop* **41**: 1561-1569. DOI: 10.1007/s00264-017-3490-6.

Omoumi P, Michoux N, Thienpont E, Roemer FW, Vande Berg BC (2015) Anatomical distribution of areas of preserved cartilage in advanced femorotibial osteoarthritis using CT arthrography (Part 1). *Osteoarthritis Cartilage* **23**: 83-87. DOI: 10.1016/j.joca.2014.10.006.

Omoumi P, Babel H, Jolles BM, Favre J (2017) Quantitative regional and sub-regional analysis of femoral and tibial subchondral bone mineral density (sBMD) using computed tomography (CT): comparison of non-osteoarthritic (OA) and severe OA knees. *Osteoarthritis Cartilage* **25**: 1850-1857. DOI: 10.1016/j.joca.2017.07.014.

Paley D, Pfeil J (2000) Prinzipien der kniegelenknahen Deformitätenkorrektur. *Der Orthopäde* **29**: 18-38. DOI: 10.1007/s001320050004.

Perilli E, Bala Y, Zebaze R, Reynolds KJ, Seeman E (2015) Regional heterogeneity in the configuration of the intracortical canals of the femoral shaft. *Calcif Tissue Int* **97**: 327-335. DOI: 10.1007/s00223-015-0014-5.

Rapagna S, Roberts BC, Solomon LB, Reynolds KJ, Thewlis D, Perilli E (2021) Tibial cartilage, subchondral bone plate and trabecular bone microarchitecture in varus- and valgus-osteoarthritis versus controls. *J Orthop Res* **39**: 1988-1999. DOI: 10.1002/jor.24914.

Reina N, Cavaignac E, Pailhé R, Pailliser A, Bonneville N, Swider P, Laffosse JM (2017) BMI-related microstructural changes in the tibial subchondral trabecular bone of patients with knee osteoarthritis. *J Orthop Res* **35**: 1653-1660. DOI: 10.1002/jor.23459.

Rivière C, Sivaloganathan S, Villet L, Cartier P, Lustig S, Vendittoli PA, Cobb J (2022) Kinematic alignment of medial UKA is safe: a systematic review. *Knee Surg Sports Traumatol Arthrosc* **30**: 1082-1094. DOI: 10.1007/s00167-021-06462-6.

Roberts BC, Solomon LB, Mercer G, Reynolds KJ, Thewlis D, Perilli E (2018) Relationships between *in vivo* dynamic knee joint loading, static alignment and tibial subchondral bone microarchitecture in end-stage knee osteoarthritis. *Osteoarthritis Cartilage* **26**: 547-556. DOI: 10.1016/j.joca.2018.01.014.

Roberts BC, Thewlis D, Solomon LB, Mercer G, Reynolds KJ, Perilli E (2017) Systematic mapping of the subchondral bone 3D microarchitecture in the human tibial plateau: variations with joint alignment. *J Orthop Res* **35**: 1927-1941. DOI: 10.1002/jor.23474.

Sacitharan PK (2019) Ageing and osteoarthritis. *Subcell Biochem* **91**: 123-159. DOI: 10.1007/978-981-13-3681-2_6.

Sampath SA, Lewis S, Fosco M, Tigani D (2015) Trabecular orientation in the human femur and tibia and the relationship with lower-limb alignment for patients with osteoarthritis of the knee. *J Biomech* **48**: 1214-1218. DOI: 10.1016/j.jbiomech.2015.01.028.

Sharma L, Song J, Felson DT, Cahue S, Shamiyeh E, Dunlop DD (2001) The role of knee alignment in disease progression and functional decline in knee osteoarthritis. *JAMA* **286**: 188-195. DOI: 10.1001/jama.286.2.188.

Shrout PE, Fleiss JL (1979) Intraclass correlations: uses in assessing rater reliability. *Psychol Bull* **86**: 420-428.

Tassani S, Perilli E (2013) On local micro-architecture analysis of trabecular bone in three

dimensions. *Int Orthop* **37**: 1645-1646. DOI: 10.1007/s00264-013-1989-z.

Wolff J (1892) *Das Gesetz der Transformation der Knochen* [The law of bone remodelling], Hirschwald, Berlin.

Wolski M, Podsiadlo P, Stachowiak GW, Lohmander LS, Englund M (2010) Differences in trabecular bone texture between knees with and without radiographic osteoarthritis detected by

directional fractal signature method. *Osteoarthritis Cartilage* **18**: 684-690. DOI: 10.1016/j.joca.2010.01.002.

Editor's note: There were no questions from reviewers for this paper; therefore, there is no Discussion with reviewers section. The Scientific Editor responsible for this paper was Stephen Ferguson.